

Susceptibility of new soil organic carbon to mineralization during dry-wet cycling in soils from contrasting ends of a precipitation gradient

Roland C. Wilhelm^{a,*}, Laurel Lynch^{a,b}, Tara M. Webster^{a,c}, Steffen Schweizer^d,
Thiago M. Inagaki^{d,e}, Malak M. Tfaily^{f,g}, Ravi Kukkadapu^f, Carmen Hoeschen^d,
Daniel H. Buckley^a, Johannes Lehmann^{a,e,h}

^a School of Integrative Plant Science, Cornell University, Ithaca, NY, 14853, USA

^b Department of Soil and Water Systems, University of Idaho, Moscow, ID, 83844, USA

^c Cooperative Institute for Research in Environmental Sciences, University of Colorado, Boulder, CO, 80309, USA

^d Chair of Soil Science, TUM School of Life Sciences, Technical University of Munich, Emil-Ramann-Straße 2, 85354, Freising, Germany

^e Institute for Advanced Study, Technical University of Munich, 85748, Garching, Germany

^f Environmental Molecular Sciences Laboratory, Pacific Northwest National Laboratory, Richland, WA, 99352, USA

^g Department of Environmental Science, The University of Arizona, Tucson, AZ, 85721, USA

^h Cornell Atkinson Center for Sustainability, Cornell University, Ithaca, NY, 14853, USA

ARTICLE INFO

Keywords:

Precipitation gradient
Carbon susceptibility
Carbon use efficiency
Iron mineralogy
NanoSIMS
Birch effect

ABSTRACT

The persistence of soil organic carbon (SOC) is influenced by soil physicochemical properties, organic matter quality, and climatic conditions that govern its vulnerability to microbial activity. We compared the susceptibility of newly formed SOC to mineralization in two soils (Andosols) that developed under contrasting precipitation regimes. Soil from the high rainfall region ('high_{rain}') had higher SOC and lower iron concentrations than soils exposed to less rainfall ('low_{rain}'). We amended soils with ¹³C-labeled carbohydrates and measured the amount of substrate-derived SO¹³C mineralized when exposed to dry-wet cycling following months-long incubations. We hypothesized that susceptibility would differ due to iron content and mineralogy, initial SOC, substrate solubility (cellulose versus glucose amendment), and microbial substrate use efficiency (SUE). We found that SO¹³C was less susceptible to dry-wet cycling when more ¹³C was assimilated into microbial biomass and co-localized with mineral surfaces than when co-localized with existing organo-mineral surfaces, according to microscale NanoSIMS imaging. Considerably less SO¹³C was susceptible to mineralization in the ferrihydrite-rich (low SOC) low_{rain} soil than the leached (high SOC) high_{rain} soil when C was added as either glucose (7.3-fold less C mineralized) or cellulose (15.2-fold less). The SUE of glucose was comparable to cellulose in low_{rain} soil where SO¹³C was less water soluble and coprecipitated with ferrihydrite, and used half as efficiently as cellulose in high_{rain} soil. Our results show that the susceptibility of newly formed SOC to mineralization is modified by the effects of bioavailability on microbial metabolism and the availability of mineral surfaces for forming new organo-mineral complexes.

1. Introduction

The persistence of soil organic carbon (SOC) depends on the physicochemical and biological factors that affect the probability and rate of mineralization (Schmidt et al., 2011; Dynarski et al., 2020; Lehmann et al., 2020). Interrelated ecosystem properties, such as climate and geochemistry, co-govern SOC susceptibility to microbial mineralization, enabling some soils to maintain higher concentrations of SOC than others (Schmidt et al., 2011; Rasmussen et al., 2018; Hall et al., 2020;

Abramoff et al., 2021; Heckman et al., 2022). Precipitation patterns regulate the bell-shaped relationship between soil moisture and decomposition rates that drive soil carbon cycling (Schoor and Matson, 2001; Derner and Schuman, 2007; Meier and Leuschner, 2010; Berthrong et al., 2012; Chang et al., 2014). While high levels of precipitation may cause SOC to accumulate, due to oxygen-limitation, higher levels of precipitation also accelerate leaching and cause the loss of mineral phases that could otherwise stabilize soil organic matter (Torn et al., 1997; Thompson et al., 2011; Kleber et al., 2015; Kramer and

* Corresponding author. School of Integrative Plant Science, 306 Tower Rd, Cornell University, Ithaca, NY, 14853, USA.

E-mail address: rcw239@cornell.edu (R.C. Wilhelm).

<https://doi.org/10.1016/j.soilbio.2022.108681>

Received 21 June 2021; Received in revised form 18 April 2022; Accepted 20 April 2022

Available online 25 April 2022

0038-0717/© 2022 Elsevier Ltd. All rights reserved.

Chadwick, 2018; Possinger et al., 2020). Feedbacks between precipitation, soil geochemistry, and microbial activity complicate the dynamics of SOC cycling, creating spatiotemporal variation in SOC persistence that is difficult to predict.

Natural precipitation gradients provide opportunities to contrast the relative influences of climate-driven soil properties on SOC persistence. Previous research at the Kohala Mountain transect, Hawai'i, demonstrated that iron and SOC concentrations co-governed the long-term persistence of SOC (Grant et al., 2022). At Kohala Mountain, subsoil OM tended to co-localize with Fe-oxides on soil particles where rainfall was low (40% of the OM in the observed areas) and far less (5% of OM) where rainfall had leached iron from soils (Inagaki et al., 2020). The age of bulk SOC was also much younger in iron-depleted soils relative to non-leached soils at equivalent depth, suggesting a link between iron mineralogy and the rate of SOC turnover. Yet, soils from higher rainfall regions had accumulated substantially more SOC, ostensibly due to more frequent water saturation and reduced rates of decomposition (Grant et al., 2022). It remains unclear how these contrasting soil properties influence the cycling of new OM inputs. Here, we used soils sourced from the Kohala transect to probe the relative importance mineralogy, SOC content, and microbial activity play in determining the susceptibility of new organic carbon inputs to mineralization.

Several biological, chemical, and thermal measures of the potential susceptibility of SOC to mineralization are used to estimate its turnover rate (Paul et al., 2006; Plante et al., 2011; Gregorich et al., 2015). Soil respiration provides the most direct measure of SOC susceptibility, but conventional respiration measurements do not capture important dynamics affecting OM turnover in soil (Six et al., 2004; Bernal et al., 2016). Soil drying and rewetting stimulates respiration, eliciting a phenomenon known as the 'Birch Effect.' Although we lack a complete mechanistic understanding of the Birch effect, major drivers include soil processes, such as SOC remobilization, organo-mineral bond dissolution, aggregate dispersion, induced mortality and biomass turnover, and the reintroduction of occluded OM and microbes (Unger et al., 2010; Evans et al., 2016; Fraser et al., 2016). Here, we used dry-wet cycling, and the resulting Birch effect, to assess SOC susceptibility to mineralization in a manner aligned with environmental exposures in mesic systems.

The efficiency by which organic carbon is converted, or sequentially cycled, into microbial biomass is an important aspect of soil OM formation that modulates the persistence of SOC (Miltner et al., 2012; Cotrufo et al., 2013; Liang et al., 2017; Woolf and Lehmann, 2019). Substrate use efficiency (SUE) can be estimated for individual carbon sources and is measured in biomass produced per unit substrate consumed ($C_{\text{biomass}}/C_{\text{biomass}} + C_{\text{respired}}$). SUE is correlated with soil moisture and organic matter quality (Manzoni et al., 2012, 2018; Öquist et al., 2017; Butcher et al., 2020), which differ across precipitation gradients (Saiz et al., 2012; Campo and Merino, 2016). Importantly, SUE can be used to approximate the efficiency of individual populations, whole communities, or as an integrated measure of the overarching influences of ecosystem properties (SUE_E) that affect carbon cycling over longer timescales, beyond the lifespan of an individual organism (Geyer et al., 2016). Here, we use SUE_E as a measure of the efficiency of microbial metabolism under environmental conditions that reflect ecosystem properties, such as soil mineralogy and resource availability.

Understanding the factors governing SOC persistence is a fundamental challenge for soil science. In this study, we investigated the susceptibility of new $SO^{13}C$ to mineralization following a months-long incubation and exposure to dry-wet cycling. We compared two soils (Andosols) that developed under contrasting precipitation regimes on Hawai'i. Soil from the lower rainfall region ('low_{rain}') had lower existing SOC and higher total iron and ferrihydrite concentrations than soil from the higher rainfall region ('high_{rain}'). Soils were incubated with either ^{13}C -labeled glucose (soluble) or cellulose (insoluble) to probe the effect of substrate bioavailability on microbial metabolism. Our objective was to evaluate several factors that influence SOC susceptibility including: (i) mineralogy, with a focus on iron minerals, (ii) SOC content, and (iii)

microbial SUE_E . We hypothesized that iron concentrations would negatively correlate with SOC susceptibility via organo-mineral interactions (Huang and Hall, 2017; Rasmussen et al., 2018; Inagaki et al., 2020). We also hypothesized that the insoluble carbohydrate (cellulose) would be cycled at a lower SUE_E than glucose, as in Öquist et al. (2017), because of the additional energy costs of enzymes required in polymer degradation (Manzoni et al., 2012). We employed high-resolution techniques (NanoSIMS) to characterize fine-scale patterns underlying differences in mineral- and organo-associated SOC. These methods allowed us to track the fate of substrate-derived carbon and to investigate the relative importance of mineral versus microbial properties affecting the susceptibility of SOC to mineralization.

2. Materials and methods

2.1. Soil collection and characterization

Representative soil samples were collected from two sites on opposite ends ('low_{rain}' and 'high_{rain}') of a precipitation gradient located within the Pu'u Eke forest reserve (20.0783 N, 155.7289 W) on the Kohala volcano (Island of Hawai'i, USA). Soils within each site possess similar properties and have been studied extensively to probe relationships among soil properties and carbon cycling (Chadwick et al., 2003; Grant et al., 2019, 2022; Inagaki et al., 2020). Mean annual temperatures ranged from 15 °C to 24 °C, and sites differed by ~400 mm of annual rainfall (Table 1), as determined using the Online Rainfall Atlas of Hawai'i (Giambelluca et al., 2013). Sites were selected based on previous work showing short-range order iron minerals were less abundant in high_{rain} sites (Kramer et al., 2012; Inagaki et al., 2020). Both soils are classified as Andosols and are derived from highly weathered, 350,000-year-old Pololu basaltic volcanic rock. Low_{rain} sites were primarily characterized by grassland vegetation with mixed ohia'ia (*Metrosideros polymorpha* Gaudich, evergreen myrtle), while high_{rain} sites were primarily forested with hapu'u *Cybotium* spp. (tree fern) and uluhe *Dicranopteris linearis* (false staghorn fern).

At each sampling site, soil profiles were excavated by hand and sampled by genetic horizon from 0.25 to 0.42 m below the soil surface (Grant et al., 2019, 2022). Samples were collected in April of 2016 and stored field-moist in plastic bags at 4 °C until analysis in February of 2017. The two soils differed in pH, total SOC, total N, the C/N ratio, $\delta^{15}N$ of total N, and $\delta^{13}C$ of total C (Table 1). Total metals in soils were measured by microwave digestion with HNO₃/HCl/HF using an Ethos Milestone Microwave Digester (methodological details in the Supporting Information, SI). Low_{rain} soil had greater amounts of iron than high_{rain} soil (26% and 14%, respectively) but similar amounts of aluminum (Table 1). An analysis of bulk soil mineralogy and iron speciation were conducted using powder X-ray diffraction (XRD) and variable temperature ^{57}Fe -Mössbauer spectroscopy (see SI for details).

Table 1

Summary of site and soil characteristics. The δ -values are expressed in per mille and correspond with the $\delta^{15}N$ of total N, $\delta^{13}C$ of total C, and $\delta^{13}C$ of microbial biomass C.

	low _{rain}	high _{rain}
Elevation (m)	1195	1520
Annu. precip. (mm)	1784.1	2286.6
Sample depth (cm)	25–35	36–42
Soil pH	6.30	4.10
Fe (%)	26.2	13.9
Al (%)	36.5	38.8
C (%)	3.94	20.25
N (%)	0.39	0.92
C/N	10.01	21.94
$\delta^{15}N$ (‰)	6.02	1.08
$\delta^{13}C$ (‰)	−21.30	−26.82
$\delta^{13}C_{MBC}$ (‰)	−27.84	−18.32

Mössbauer spectroscopy was also used to identify the composition of crystalline Fe-oxide mineral oxide suite, the nature of ferrihydrite-organic matter coprecipitates, and Fe-containing silicate minerals, according to previously described methods (Eusterhues et al., 2008; Chen et al., 2015; Noor and Thompson, 2022).

2.2. Soil microcosm experiment

Three replicate soil microcosms were prepared for each soil by adding 12 g dry weight (d.w.) field soil to 60-mL serum vials and adjusting to 50% water holding capacity (WHC). Microcosms were pre-incubated at room temperature (23 °C) for one week to minimize any initial differences in the concentration of easily mineralizable SOC. Soils were then amended at a rate of 0.3 mg C per g d.w. soil (~0.8% increase in total SOC) with ^{13}C -labeled glucose (99 atom % ^{13}C ; Sigma-Aldrich) or bacterial cellulose (99 atom % ^{13}C), manufactured as previously described (Pepe-Ranney et al., 2016). After amendment, microcosms were vortexed at low intensity for ~5 s to mix soil and carbohydrate substrate, then crimp sealed with rubber stoppers and incubated at 23 °C in the dark. Respiration was monitored by sampling headspace approximately every 12 h (glucose) or 24 h (cellulose) until the production of $^{13}\text{CO}_2$ subsided, and then at diminishing intervals from every 1–3 days. Using a gas-tight syringe, 200- μL of headspace gas was transferred into evacuated 2-mL vials and analyzed by GC/MS (Shimadzu GCMS-QP2010S), and the headspace was flushed with filtered air after each sampling. The quantity of $^{12}\text{CO}_2$ (m/z 44) and $^{13}\text{CO}_2$ (m/z 45) was determined by GC-MS using a set of standards. Contributions to $^{13}\text{CO}_2$ from the natural abundance of ^{13}C present in existing SOC were subtracted based on estimations from the net $^{12}\text{CO}_2$ and $\delta^{13}\text{C}$ of SOC in each soil. The expected variation in natural ^{13}C abundance among SOC pools was negligible relative to the enrichment level of ^{13}C derived from our uniformly ^{13}C -labeled substrates. Initial incubations were concluded once the rate of $^{13}\text{CO}_2$ respiration was similar across a three-day period between low_{rain} and high_{rain} soil, according to each substrate: ~42 days for glucose and 88–110 days for cellulose.

2.3. SOC susceptibility test

At the end of the incubation period, 5 g (d.w.) of each sample were transferred to a new serum vial and subjected to three consecutive rounds of dry-wet cycling to test SOC susceptibility. We define the susceptibility of substrate-derived SO^{13}C as the net amount of $^{13}\text{CO}_2$ produced during the 72 h post-wetting of each cycle. Specifically, the higher the net $^{13}\text{CO}_2$ flux produced in the period following the three consecutive drying and re-wetting cycles – the more susceptible the SO^{13}C . For each dry-wet cycle, microcosms were air dried in a laminar flow hood for 24 h (to 25–30% WHC) and rewetted back to 50% WHC. The amount of $^{13}\text{CO}_2$ produced was measured using the sample methods described above. The net $^{13}\text{CO}_2$ respired following dry-wetting was normalized to the amount of substrate ^{13}C remaining in the soil, which was calculated from the cumulative $^{13}\text{CO}_2$ respired at the end of the initial experiment. Each subsequent dry-wet cycle was initiated when the rate of $^{13}\text{CO}_2$ flux had reached background levels prior to initiating drying, which was comparable among each soil type and substrate amendment (~12 additional hrs).

2.4. Microbial substrate use efficiency

Microbial biomass carbon and nitrogen were calculated as the difference between paired chloroform-fumigated and non-fumigated subsamples, as previously described (Lynch et al., 2018). Total C and $\delta^{13}\text{C}$ were measured using lyophilized extracts run on an elemental analyzer (Carlo Erba NC2500, Lancanshire, UK) coupled to an isotope-ratio mass spectrometer (Finnigan MAT Delta Plus; Thermo Electron Corporation, Bremen, Germany) at the Cornell University Stable Isotope Laboratory. We applied a two-source mixing model (Post, 2002) to assess the relative

contribution of native SO^{12}C versus ^{13}C -cellulose or ^{13}C -glucose to microbial biomass C as described in SI. Microbial SUE, estimated as an ecosystem property (SUE_E ; Geyer et al., 2016) and defined by the partitioning of ^{13}C substrate between growth and respiration:

$$\text{equation } \text{SUE}_E = \frac{^{13}\text{MB}}{(^{13}\text{MB} + ^{13}\text{CO}_2)}$$

Where ^{13}MB represents the fraction of ^{13}C -substrate assimilated in microbial biomass ($\text{g} \bullet \text{C g d.w. soil}^{-1}$), and $^{13}\text{CO}_2$ represents the fraction of ^{13}C -substrate converted to CO_2 ($\text{g} \bullet \text{C g d.w. soil}^{-1}$) at the end of the incubation period for each substrate and soil. We did not measure the K_{ec} of these soils directly and therefore did not apply a correction factor following previous recommendations (Dictor et al., 1997; Weintraub et al., 2007).

2.5. Analysis of water-soluble and iron-associated carbon

Total dissolved organic C (DOC) concentrations were determined for 2 g d.w. soil of pre- and post-incubation soils as previously described (Weintraub et al., 2007) with full details in the SI. DOC was measured using a Shimadzu TOC-L (Shimadzu Scientific Instruments, Inc. Kyoto, Japan). At the end of the incubation, iron-associated SOC was extracted from microcosm soils using oxalate or hydroxylamine hydrochloride (HH; Coward et al., 2017) with KCl as reference. Oxalate and HH dissolve iron minerals, but unlike oxalate, HH is not C based, permitting downstream C analyses. Soils were finely ground with a mortar and pestle and extracted at a 1:40 ratio with either 0.25 M HH, 0.2 M ammonium oxalate (adjusted to pH 3 with 0.2 M oxalic acid), or 0.2 M KCl. Soil solutions were shaken for 4 h (180 rpm), centrifuged for 20 min at 1000 rpm, and filtered through 0.45- μm glass fiber filter papers (Advantec GC-50). Total DO^{13}C and DO^{12}C were measured in HH and KCl extracts at the UC Davis Stable Isotope Facility. Oxalate extracts were not measured due to the confounding effects of oxalate-C. The recovery of iron and aluminum for all extracts was measured by Inductively Coupled Plasma Atomic Emission Spectrometry with a Thermo iCAP 6500 (Thermo Fischer Scientific, Waltham, MA).

2.6. Determining mineral- and organo-associated SO^{13}C with NanoSIMS

After incubation, the microscale localization of ^{13}C on soil particles was imaged using a NanoSIMS 50L instrument (CAMECA, Gennevilliers, France) at the Technical University of Munich. Soil particles were deposited on Si wafers where regions of interest (30 \times 30 μm), containing between one and five microaggregates (~5–20 μm diameter), were randomly identified using SEM imaging. Four to eight regions of interest were scanned per sample, with an average of 67 microaggregates imaged per treatment. Regions were rasterized with the Cs^+ primary ion beam (ca. 2 pA) with an ion impact energy of 16 keV and spot size of ~150 nm. We measured the secondary ions of $^{12}\text{C}^-$, $^{13}\text{C}^-$, $^{16}\text{O}^-$, $^{12}\text{C}^{14}\text{N}^-$, $^{27}\text{Al}^{16}\text{O}^-$, and $^{56}\text{Fe}^{16}\text{O}^-$ during scanning. The instrument was tuned at high mass resolution to separate mass isobars accurately (e.g., $^{13}\text{C}^-$ versus $^{12}\text{C}^{16}\text{O}^-$). Secondary ions that escaped the sample surface were recorded using a dwell time of 1 ms \cdot pixel $^{-1}$ with 256 \times 256 pixels for a 30 \times 30 μm field of view and 40 planes per measurement. Details on sample preparation, NanoSIMS imaging, and total particles/surface area imaged are provided in the SI. Data were normalized to total particle area since the total particle area imaged differed due to natural variation in particle sizes (Table S1).

A control sample containing non-amended field soil was measured for each sample to account for instrument stability and instrumental fractionation. The NanoSIMS measurements were analyzed using image analysis and multi-channel machine-learning segmentation that integrated a variety of image features (i.e., intensity, texture and gradient) in all isotope distributions (Fig. S1), as previously described (Schweizer et al., 2018). This enabled identification and quantification of non-enriched, native OM (yielding high counts for C and N species), the

native OM associated with the amended ^{13}C -enriched substrate (OM co-localized ^{13}C), as well as mineral-dominated surfaces with substrate-derived ^{13}C enrichment (mineral co-localized ^{13}C). Segmentation was used to quantify the overlap of ^{13}C -enriched spots with mineral-dominated and OM-dominated surfaces (Fig. S1e). Further details about image processing and segmentation are provided in the SI.

2.7. Statistical analyses

All statistical analyses were performed in R (v. 3.4.0) using ANOVA ('aov'), for comparison among multiple factors; Tukey HSD ('TukeyHSD') for pairwise contrasts among multiple factors; t-tests ('t.test') for contrasts between two factors, and the Wilcoxon test ('wilcox.test') when contrasting two factors that did not meet the expectations of normality.

3. Results

3.1. Soil mineralogy and iron composition

According to XRD, both the $\text{high}_{\text{rain}}$ and low_{rain} soils were a mixture of quartz (the dominant crystalline mineral phase), hematite, maghemite, ulvospinel, ilmenite, anorthite and amorphous or poorly crystalline minerals of varying composition (Fig. S2). low_{rain} soil had a higher

proportion of poorly crystalline minerals and broad spectral features concurring with XRD spectra of pure ferrihydrite (Kukkadapu et al., 2003), with interference from amorphous aluminosilicate minerals typical of volcanic soils. Mössbauer spectroscopy measurements confirmed that both soils were contained varying mixtures of hematite, goethite, maghemite, ulvospinel, ilmenite ($\text{high}_{\text{rain}}$ only), Fe-containing silicates (anorthite), and ferrihydrite-like mineral phases (Fig. S3). Spectral modeling indicated that 73% (low_{rain}) and 51% ($\text{high}_{\text{rain}}$) of the total iron pool was ferrihydrite-like, and coprecipitated with SOM at varying C:Fe ratios. In general, the C:Fe ratio in the low_{rain} soil was relatively higher than the $\text{high}_{\text{rain}}$ soil. The composition of the remaining portions of Fe (12–20%) could not be resolved due to the overlapping spectra of phyllosilicates, feldspars, and pyroxenes.

3.2. Respiration and SUE_E

Initial substrate respiration rates ($^{13}\text{CO}_2$) were higher from low_{rain} than $\text{high}_{\text{rain}}$ soils (Fig. 1). After a lag of three days, the amount of ^{13}C -glucose respired from $\text{high}_{\text{rain}}$ soils surpassed low_{rain} soils, and a greater proportion of the total substrate was ultimately respired (48% from $\text{high}_{\text{rain}}$ versus 39% from low_{rain} , Fig. 1a). The total proportion of ^{13}C -cellulose respired (~30%) was lower than glucose in both soils. Overall, the respiration of native SOC (i.e., SO^{12}C) was greater in $\text{high}_{\text{rain}}$ than low_{rain} soils (Fig. 1b). After approximately 60 days, more native SO^{12}C

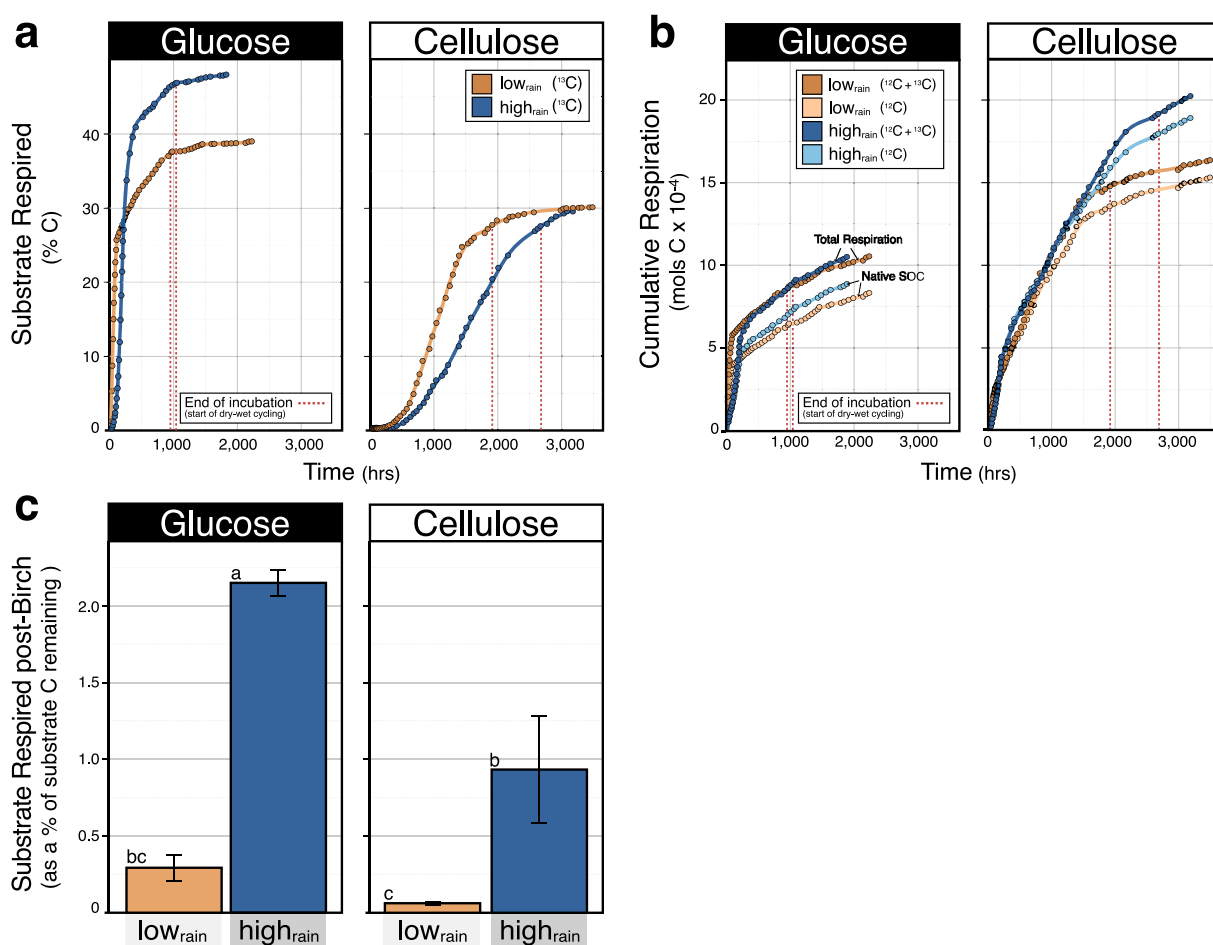


Fig. 1. Soil amendments of ^{13}C -glucose and ^{13}C -cellulose were mineralized at different rates in low_{rain} and $\text{high}_{\text{rain}}$ soils. Panel (a) displays the proportion of substrate respired (according to headspace measurements of $^{13}\text{CO}_2$), while panel (b) displays total cumulative respiration, which includes the mineralization of native SOC ($^{12}\text{CO}_2$). The persistence of substrate-derived (^{13}C) was lower in $\text{high}_{\text{rain}}$ soils, based on (c) the cumulative $^{13}\text{CO}_2$ respired in the 72-hr period following three dry-wet cycles normalized to the % of unrespired substrate C. In (a) and (b), the x-axis corresponds to the length of incubation (marked with a red dotted line) plus the period of dry-wet cycling. All analyses were performed on soils sampled at the end of the incubation. In (c), lettering denotes significant differences according to Tukey's HSD test ($p < 0.05$). For reference, 1000 h is approximately 42 days. (For interpretation of the references to color in this figure legend, the reader is referred to the Web version of this article.)

was respired from cellulose- than glucose-amended soils, producing 1.8- and 2.1-fold more $^{12}\text{CO}_2$ flux from cellulose-amended low_{rain} and high_{rain} soils, respectively (Fig. 1b). Initial microbial biomass was an order of magnitude greater in low_{rain} than high_{rain} soils (Table 2), consistent with higher initial rates of respiration. SUE_E was higher for both substrates in the low_{rain} soils, and a greater proportion of substrate-derived ^{13}C was assimilated into biomass in low_{rain} soil. While SUE_E was comparable between substrates in low_{rain} soils, cellulose was consumed with a higher SUE_E than glucose in high_{rain} soils (0.4 versus 0.2, respectively). Overall, SUE_E was more variable between replicates in soils amended with cellulose than glucose.

3.3. Susceptibility of SO^{13}C

The susceptibility of substrate-derived SO^{13}C was measured based on the net $^{13}\text{CO}_2$ respired following three dry-wet cycles. More $^{13}\text{CO}_2$ was respired from high_{rain} than low_{rain} soils, indicating a greater susceptibility of new SO^{13}C to mineralization (Fig. 1c). High_{rain} soils amended with glucose were most susceptible to mineralization, with more $^{13}\text{CO}_2$ produced during dry-wet cycling than any other treatment, despite having the highest amount of substrate mineralized prior to dry-wet cycling (Fig. 1a). Differences in susceptibility were greater between soil types (ANOVA; $F_1 = 82$; $p < 0.001$) than between substrates, with cellulose-derived SO^{13}C less susceptible than glucose-derived SO^{13}C (ANOVA; $F_1 = 23$, $p = 0.001$). Soils with the most microbial biomass (Table 2) at the end of incubation also had the least susceptible SO^{13}C , as indicated by their low $^{13}\text{CO}_2$ production in response to rewetting (Fig. 1c).

3.4. Iron-associated and water-soluble SO^{13}C

Contrary to our expectation that HH and oxalate would dissolve similar amounts of iron (Coward et al., 2017), HH solubilized far less iron and aluminum than oxalate (Fig. 2). The ^{13}C enrichment of water-soluble and iron-associated solubilized SO^{13}C (in HH extracts) was highest in glucose-amended high_{rain} soils (Fig. 3). Total extractable DOC was also greater in high_{rain} soils (Wilcoxon test, $p < 0.001$, Fig. S4).

3.5. Spatial co-localization of SO^{13}C

The co-localization of SO^{13}C with mineral- and OM-dominated surfaces was imaged using NanoSIMS (Fig. 4a; Fig. S1). Large differences in OM-dominated surfaces were observed between high_{rain} soil (40% OM-dominated) and low_{rain} soil (14% OM-dominated; Fig. 4b). Low_{rain} soils amended with glucose had the greatest co-localization of ^{13}C with mineral surfaces (Fig. 4c) and the least susceptible SO^{13}C (Fig. 1c). In high_{rain} soils, most ^{13}C was co-localized with OM-dominated surfaces, reflecting a higher abundance of OM-dominated relative to mineral surfaces (Fig. 4c). More glucose- than cellulose-derived ^{13}C was co-localized with mineral surfaces in both soils. Cellulose additions resulted in lower proportions of ^{13}C -enriched surfaces than glucose, suggesting less association of the added substrate with the microaggregates analyzed by NanoSIMS.

Table 2

Microbial biomass measurements and substrate use efficiency (SUE_E). All values are the average of replicate soil microcosms. Higher variability in cellulose SUE_E was apparent in the higher standard deviations (\pm). Direct comparison of SUE_E between glucose-amended high_{rain} and low_{rain} soils is possible, since both were incubated for 42-days. Given the unequal incubation length of soils for other conditions, comparison should be interpreted with caution, since SUE_E is expected to decline over time through biomass recycling. Lettering denotes significant differences between high_{rain} and low_{rain} soils for each measurement according to t-tests ($p < 0.05$).

	Initial Biomass (mg C g ⁻¹ dry soil)	Final Biomass (mg C g ⁻¹ dry soil)		Substrate-derived Biomass ($\mu\text{g}^{13}\text{C g}^{-1}$ dry soil)		Substrate Use Efficiency (SUE)	
		Glucose	Cellulose	Glucose	Cellulose	Glucose	Cellulose
low _{rain}	1.13 ^b ± 0.13	1.18 ^b ± 0.35	1.06 ± 0.65	0.58 ^b ± 0.13	0.44 ± 0.25	0.59 ^b ± 0.05	0.56 ± 0.19
high _{rain}	0.14 ^a ± 0.01	0.18 ^a ± 0.06	0.48 ± 0.40	0.13 ^a ± 0.05	0.38 ± 0.40	0.22 ^a ± 0.08	0.44 ± 0.29

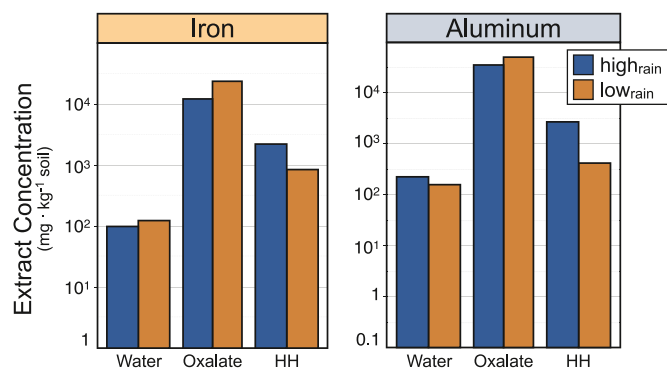


Fig. 2. A comparison of the metal extraction efficacy of oxalate and hydroxylamine hydrochloride (HH) metal-solubilizing soil treatments. Iron and aluminum concentrations in oxalate and HH extracts were compared against water extracts and a saline control extract (KCl). Metal-solubilizing extractions were used to compare the amount of ^{13}C associated with iron/aluminum in high_{rain} and low_{rain} soils. The HH-based extraction was preferred, since HH is not carbon based. Bars are colored by soil type. Duplicate measurements were made for water and oxalate extractions with bars representing the average.

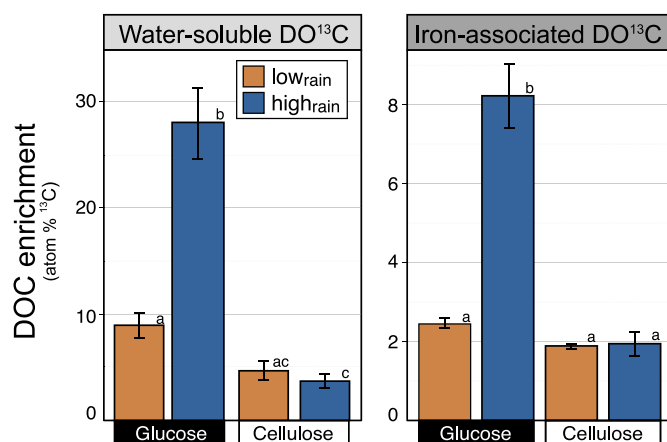


Fig. 3. The addition of ^{13}C -glucose to high_{rain} soil resulted in a significant increase in extractable SO^{13}C at the end of the incubation relative to low_{rain} soils and soils to which ^{13}C -cellulose was added. DO^{13}C was determined on the basis of atom % ^{13}C enrichment of lyophilized DOC derived from water soluble (KCl) and iron-associated (hydroxylamine hydrochloride; HH) fractions. The mass of soil extracted was the same across samples and conditions. Lettering denotes significant differences according to Tukey's HSD test ($p < 0.05$).

4. Discussion

Soils with differing edaphic properties (iron mineralogy and total SOC) were selected to evaluate the susceptibility of newly formed SO^{13}C to microbial activity in a soil microcosm experiment. Sourced from contrasting ends of a natural precipitation gradient, these soils capture differences in pedological development, but were not intended to assess variation at the ecosystem scale or by depth. Soluble (^{13}C -glucose) and

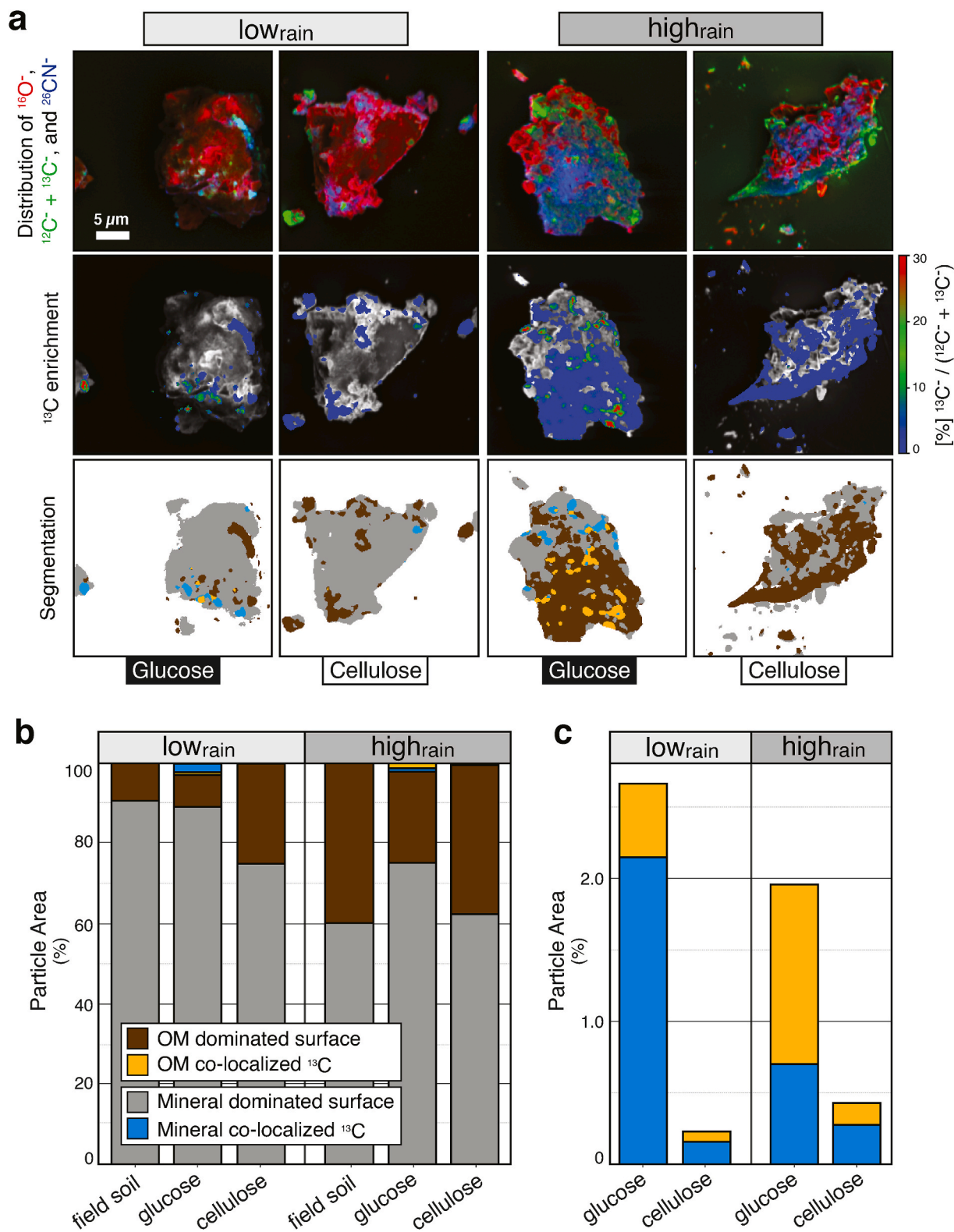


Fig. 4. Spatial analysis of the co-localization of SO^{13}C with OM- versus mineral-dominated surfaces using NanoSIMS. In (a), examples of imaged microaggregates illustrating differences in co-localization among low_{rain} and $\text{high}_{\text{rain}}$ soils incubated with ^{13}C -labeled glucose or cellulose. In (b), differences in the proportion of OM-dominated surfaces are apparent in the segmentation of particle surface area average across 4 to 8 images per treatment and substrate. In (c), a close-up view of the proportion of SO^{13}C co-localized with mineral- and OM-dominated surfaces between low_{rain} $\text{high}_{\text{rain}}$, respectively, from data shown in (b). In (a), the first row of images displays the distribution of O, C, and N in RGB coloring. The second row displays the atom % ^{13}C enrichment as a heatmap of ^{13}C -enriched and OM-dominated surfaces with the equally scaled $^{16}\text{O}^{-} + ^{26}\text{CN}^{-}$ distribution showing the particle surface structure in grey. The third row displays the segmentation mask produced by multichannel machine-learning. Further details on the image analysis are provided in the SI and Fig. S1.

insoluble (^{13}C -cellulose) substrate was added to each soil and mineralization was measured over several months. We compared the susceptibility of SO^{13}C (i.e., the ^{13}C remaining after substrate respiration had subsided) by measuring the net $^{13}\text{CO}_2$ respired following three rounds of dry-wet cycling. We found that SO^{13}C was less susceptible to dry-wet cycling in soil from the lower rainfall region, which had higher iron content, higher SUE_E , lower pre-existing SOC, and a greater proportion of SO^{13}C co-localized with mineral surfaces (Fig. 5). Conversely, $\text{high}_{\text{rain}}$ soil had lower iron content, a higher proportion of mineral surfaces complexed with native OM, and more of the newly derived SO^{13}C was susceptible to mineralization. These findings stress the importance of mineral surfaces for stabilizing SOM inputs (Kleber et al., 2007) and suggest OM-OM bonds are weaker than OM-mineral bonds. These findings support our hypothesis that microbial activity and underlying mineralogy influence the susceptibility of recently formed SOC to dry-wet cycling.

4.1. The impact of climate on soil properties and SOC susceptibility

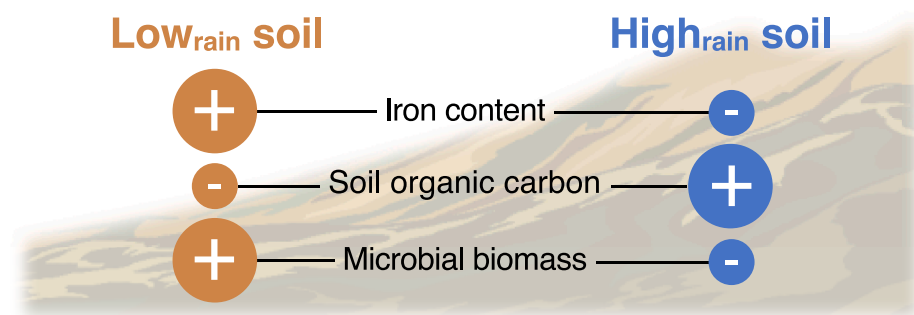
Low_{rain} soils had more total iron and ferrihydrite, while iron in $\text{high}_{\text{rain}}$ soils was more reduced, consistent with expectations that higher precipitation would lead to water saturation and iron leaching (Thompson et al., 2011; Inagaki et al., 2020). Low_{rain} soils had high concentrations of amorphous/poorly crystalline ferrihydrite, a greater development of ferrihydrite-OM coprecipitates, and more SO^{13}C co-localized with mineral surfaces. These properties corresponded with a reduced susceptibility of SO^{13}C to mineralization, which was lowest in

low_{rain} soil, suggesting iron-containing minerals (here, ferrihydrite) promote persistence by protecting SOC from mineralization (Rumpel and Kögel-Knabner, 2011; Kaiser and Kalbitz, 2012). Our findings are consistent with previous research at the site, linking aluminum and iron oxides with C-stabilization in regions of lower precipitation (Inagaki et al., 2020).

Our findings suggest that newly formed SOC is less susceptible to microbial degradation when associated with mineral-dominated surfaces than when associated with pre-existing OM. Although $\text{high}_{\text{rain}}$ soils contained 5-fold more SOC than low_{rain} soils, a greater proportion of SO^{13}C was co-localized with OM dominated surfaces and more prone to mineralization. Approximately 7.3- (glucose) and 14.7-fold (cellulose) more SO^{13}C was respired from $\text{high}_{\text{rain}}$ than low_{rain} following dry-wet cycling. Notably, the increased susceptibility of SO^{13}C in $\text{high}_{\text{rain}}$ soil was observed even though ~60% of mineral-dominated surfaces were free of OM. This result supports the tendency of new C to co-localize with existing SOC, leading to greater susceptibility to turnover (Vogel et al., 2014; Schweizer et al., 2018). The higher proportion of mineral surface and reactive minerals, like ferrihydrite, in low_{rain} soil appears to reduce the probability of new SO^{13}C associating with existing SOC. Thus, spatial differences in microscale co-localization of substrate with OM- or mineral-dominated surfaces can be a factor driving OM turnover.

Our method for measuring SO^{13}C susceptibility to mineralization, using dry-wet cycling, was chosen to reflect a naturally occurring process termed the Birch effect. The combined influence of biomass, microbial activity and growth dynamics govern the intensity of effect (Unger et al., 2010; Evans et al., 2016; Fraser et al., 2016). Consistent

Properties of Soils from Precipitation Gradient



Summary of Experimental Results

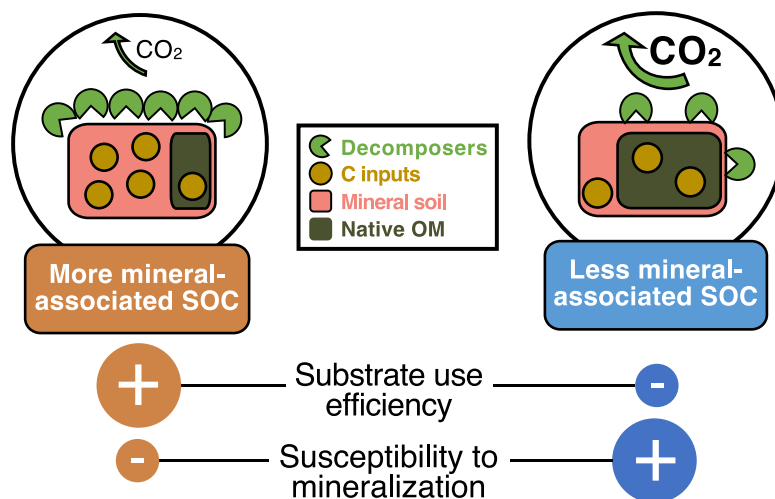


Fig. 5. A graphical summary of results illustrating differences in soil mineral properties, SOC formation, microbial biomass and SUE of the soils from high and low rainfall regions of our precipitation gradient. Overall, our evidence suggests that the persistence of substrate-derived SO^{13}C was enhanced by assimilation into microbial biomass and by association with mineral surfaces. These effects were pronounced in low_{rain} soils, where SO^{13}C was most persistent.

with past findings from precipitation gradients (Manzoni et al., 2012; Butcher et al., 2020), initial microbial biomass and SUE_E differed substantially between our two soils, demonstrating SUE_E was affected by precipitation-related environmental controls. The most susceptible $SO^{13}C$ (i.e., greatest Birch effect) coincided with the highest recovery of water-soluble and iron-associated $SO^{13}C$ in high_{rain} soil, rewetting increased $SO^{13}C$ remobilization by dissolution of organo-mineral bonds and/or dispersing aggregates (Six et al., 2004; Bernal et al., 2016). The extent to which dry-wet cycling can serve as a comprehensive test of SOC susceptibility to mineralization requires further testing. For example, results may be decoupled in systems where dry-wet cycling occurs infrequently (i.e., arid, permafrost, or high-precipitation environments). We therefore require a more mechanistic understanding of the Birch effect to assess its efficacy as a comprehensive measure of SOC susceptibility.

4.2. SUE_E and $SO^{13}C$ susceptibility

We observed the lowest susceptibility of $SO^{13}C$ where conditions facilitated efficient microbial-processing of new ^{13}C -substrates. Microbial communities in low_{rain} soils had the highest relative SUE_E (0.6) and least susceptible $SO^{13}C$ for both substrates. Communities inhabiting high_{rain} soils utilized cellulose with a relatively high SUE_E (0.4) and microbial processing of cellulose corresponded with significantly lower susceptibility of $SO^{13}C$. These results suggest that soil conditions favoring high SUE_E should diminish the susceptibility of SOC to mineralization and promote SOC persistence, supporting prior evidence (Kallenbach et al., 2015).

We also compared the effect of substrate bioavailability on SUE_E using two model carbohydrates, glucose (soluble) and cellulose (insoluble), that are metabolized through the same central metabolism of cells. We hypothesized that glucose would yield higher SUE_E than cellulose based on a prior comparison (Öquist et al., 2017) and the expected influence of the energetic costs of extracellular enzyme production (Manzoni et al., 2012), but observed the opposite result. The disparity with Öquist et al. (2017) may reflect differences in incubation length (eight days versus several months), since measuring SUE over longer periods integrates a broader range of soil properties that affect efficiency, such as changes in environmental conditions, resources, and the diversity and succession (biomass turnover) of microbial communities (Manzoni et al., 2012; Geyer et al., 2016, 2020; Domeignoz-Horta et al., 2020; Buckeridge et al., 2022). Yet, our result is consistent with the finding that glycogen, a branched glucose polymer, was metabolized at higher SUE than glucose in soil even when incubations were short (32 h; Bölscher et al., 2016), and with the general observation that SUE decreases when substrate bioavailability increases, as shown in the lower SUE of glucose at higher soil amendments (Schneckenberger et al., 2008).

Relative differences in SUE_E and $SO^{13}C$ susceptibility to mineralization likely result from differences in growth strategies employed by microorganisms encountering substrates with varying degrees of bioavailability (Barnett et al., 2022). In general, slower-growing microbial communities exhibit higher SUE (Roller and Schmidt, 2015); therefore, it stands to reason that slower-growing, cellulose-degrading populations would exhibit higher SUE_E , since the processing rates of extracellular enzymes limit growth. Conversely, the lower SUE_E exhibited during the metabolism of glucose illustrates the relatively higher energetic costs associated with zymogenous growth relative to extracellular enzyme activity (Manzoni et al., 2012). We observed this trend despite cellulose-amended soils incubating for significantly longer than glucose-amended soils (+46–64 days), which we expect would reduce SUE_E through sequential biomass turnover.

Alternatively, it is possible the initial assimilation of cellulosic-C into biomass occurred more gradually than glucose, offsetting differences in turnover from longer incubations, as suggested by the substrate respiration curves in Fig. 1A. In this case, the comparable SUE_E observed for

glucose and cellulose in low_{rain} soils is unexpected. According to Mössbauer and NanoSIMS results, we speculate that the bioavailability of glucose C may have decreased due to co-localization with ferrihydrite-rich mineral surfaces, leading to similar SUE_E as cellulose. Conceivably, the degradation of mineral-associated $SO^{13}C$ requires similar adaptations as those required for accessing insoluble organic matter, such as a dependence on extracellular enzymes. This could explain why ferrihydrite-rich soil selected for specialized surface-adhering bacteria (e.g., *Caulobacter*) in a study comparing the influence of mineral types on rhizodeposition (Whitman et al., 2018). Hence, organo-mineral interactions may favor specialized microbial communities with slower growth rates and higher SUE_E even when soluble C is added.

Differences in the initial microbial biomass between our soils may have also affected SUE_E . Soils with more biomass tend to consume added glucose at a higher SUE , generating more stable $SO^{13}C$ (Geyer et al., 2020), consistent with our findings, where low_{rain} soil amended with glucose had the highest starting biomass, greatest SUE_E , and lowest $SO^{13}C$ susceptibility. Similarly, microbial communities sourced from regions with historically low precipitation tend to have higher SUE (Buckeridge et al., 2020). It is important to note that our method for measuring SUE_E did not measure the contribution of microbial residues (i.e., non-biomass SOC) to the efficiency quotient, which can be significant (Geyer et al., 2020; Shao et al., 2021), nor could it resolve the effects of biomass recycling over time.

4.3. Respiration of native SOC

While the primary aim of our study was to investigate how climate and soil properties affect the susceptibility of newly formed $SO^{13}C$ to mineralization, we observed differences in the rate turnover of pre-existing SOC between substrates. Relative to glucose, cellulose amendment produced two-fold greater mineralization of existing $SO^{12}C$, resulting in the mineralization of 600 and 1000 $\mu g C \cdot g^{-1} d.w.$ in low_{rain} and high_{rain} soils, respectively. Without water-only controls, we cannot determine whether cellulose amendment elicited a positive priming response or whether glucose suppressed decomposition rates. Yet, the difference in $SO^{12}C$ mineralized between cellulose-amended soils was far greater than the amount of negative priming expected from glucose, which ranges between 10 and 50 $\mu g g^{-1} d.w.$ soil (Mason-Jones and Kuzyakov, 2017), and was within the upper ranges of positive priming reported from cellulose (450 $\mu g g^{-1} d.w.$ soil; Perveen et al., 2019). Notably, the addition of cellulose caused the greatest mineralization of pre-existing SOC from high_{rain} soil which had a higher initial SOC concentration.

Paradoxically, we found that both substrate-derived and native SOC were most susceptible to mineralization during dry-wet cycling in soils with the greatest natural accumulation of SOC. The susceptibility of SOC in high_{rain} soil coincided with lower initial microbial biomass, lower SUE_E , and lower iron content. These results suggest the accumulation of SOC at the high_{rain} site was driven by prevailing climatic conditions that govern primary production and microbial activity dynamics, namely the control of moisture on decomposition rates. However, experimental perturbation revealed the susceptibility of newly added C to dry-wet cycling, possibly resulting from the tendency of new SOC to associate with existing OM-dominated surfaces and from less efficient substrate assimilation into microbial biomass.

5. Conclusions

We characterized the relationships between SOC susceptibility to mineralization during dry-wet cycling and climate-driven changes in soil physicochemical and biological properties using two soils from contrasting ends of a precipitation gradient. $SO^{13}C$ derived from the microbial processing of ^{13}C -substrates was more stable in soil from the low rainfall region, where substrates were more likely to be converted

into microbial biomass and associated with mineral surfaces (Fig. 5). We attribute these trends to differences in the bioavailability of SO^{13}C , which governed differences in microbial metabolism and substrate use efficiency, and which were linked to the likelihood of stabilization via organo-mineral associations. Our findings suggest that the susceptibility of SOC to mineralization is governed by coupled processes that link microbial metabolism with the physicochemical protection of soil carbon.

Author contributions

RCW contributed to the overall study design, specifically the susceptibility assay, and performed data analysis, research, and writing. LL contributed to the overall study design, measured SUE, performed data analysis, and made major contributions to writing. TMW contributed to the overall study design, coordinated experiments, performed data analysis, and made major contributions to research and writing. SAS performed NanoSIMS imaging and data analysis and contributed to writing. TMI performed NanoSIMS and data analysis and prepared Fig. 5. MT contributed to data analysis. RK performed the Mössbauer analysis and interpretation. CH performed NanoSIMS analysis and interpretation. DHB and JL guided all research efforts, including study design, analyses, interpretation, and writing.

Declaration of competing interest

The authors declare that they have no known competing financial interests or personal relationships that could have appeared to influence the work reported in this paper.

Acknowledgements

This work was supported by the U.S. Department of Energy (DOE) Office of Biological & Environmental Research Genomic Science Program under award number DE-SC0016364. We acknowledge the support of Ingrid Kögel-Knabner and the Technical University Munich – Institute for Advanced Study, funded by the German Excellence Initiative (and the EU Seventh Framework Programme under grant agreement n° 291763). We thank the German Research Foundation (DFG) for the financial support for the NanoSIMS instrument (KO 1035/38–1). We thank Katherine Grant and Louis A. Derry for providing soil samples. We are grateful to Rosalie Chu, Kelly Hanley, and Mark Bowden for running FT-ICR-MS, extractions, and XRD, respectively. FTICR-MS was supported by the DOE Office of Science Graduate Student Research (SCGSR) program awarded to LML, administered by the Oak Ridge Institute for Science and Education (ORISE) under contract number DE-SC0014664. Mössbauer spectroscopy and XRD was performed at the Environmental Molecular Sciences Laboratory (User Proposal 47803) which is part of the DOE at the Pacific Northwest National Laboratory.

Abbreviations

DOC	dissolved organic carbon
HH	hydroxylamine hydrochloride
high _{rain}	field site receiving highest levels of precipitation
low _{rain}	field site receiving lowest levels of precipitation
MB	microbial biomass
NanoSIMS	nanoscale secondary ion mass spectrometry
SOC	soil organic carbon
SO^{13}C	soil organic carbon derived from ^{13}C -labeled substrate
SUE	microbial substrate use efficiency
SUE _E	a SUE measurement over long periods of time - integrates broader environmental influences
OM	organic matter
XRD	X-ray diffraction.

Appendix A. Supplementary data

Supplementary data to this article can be found online at <https://doi.org/10.1016/j.soilbio.2022.108681>.

References

- Abramoff, R.Z., Georgiou, K., Guenet, B., Torn, M.S., Huang, Y., Zhang, H., Feng, W., Jagadamma, S., Kaiser, K., Kothawala, D., Mayes, M.A., Ciais, P., 2021. How much carbon can be added to soil by sorption? *Biogeochemistry* 152, 127–142. <https://doi.org/10.1007/s10533-021-00759-x>.
- Barnett, S.E., Youngblut, N.D., Koechli, C.N., Buckley, D.H., 2022. Multi-substrate DNA Stable Isotope Probing Reveals Guild Structure of Bacteria that Mediate Soil Carbon Cycling. *PNAS*.
- Bernal, B., Mckinley, D.C., Hungate, B.A., White, P.M., Mozdzer, T.J., Magonigal, J.P., 2016. Limits to soil carbon stability; Deep, ancient soil carbon decomposition stimulated by new labile organic inputs. *Soil Biology and Biochemistry* 98, 85–94. <https://doi.org/10.1016/j.soilbio.2016.04.007>.
- Berthrong, S.T., Piñeiro, G., Jobbágy, E.G., Jackson, R.B., 2012. Soil C and N changes with afforestation of grasslands across gradients of precipitation and plantation age. *Ecological Applications* 22, 76–86. <https://doi.org/10.1890/10-2210.1>.
- Bölscher, T., Wadsö, L., Börjesson, G., Herrmann, A.M., 2016. Differences in substrate use efficiency: impacts of microbial community composition, land use management, and substrate complexity. *Biology and Fertility of Soils* 52, 547–559. <https://doi.org/10.1007/s00374-016-1097-5>.
- Buckeridge, K.M., Creamer, C., Whitaker, J., 2022. Deconstructing the microbial necromass continuum to inform soil carbon sequestration. *Functional Ecology* 1–15. <https://doi.org/10.1111/1365-2435.14014>.
- Buckeridge, K.M., Mason, K.E., McNamara, N.P., Ostle, N., Puissant, J., Goodall, T., Griffiths, R.I., Stott, A.W., Whitaker, J., 2020. Environmental and microbial controls on microbial necromass recycling, an important precursor for soil carbon stabilization. *Communications Earth & Environment* 1, 1–9. <https://doi.org/10.1038/s43247-020-00031-4>.
- Butcher, K.R., Nasto, M.K., Norton, J.M., Stark, J.M., 2020. Physical mechanisms for soil moisture effects on microbial carbon-use efficiency in a sandy loam soil in the western United States. *Soil Biology and Biochemistry* 150, 107969. <https://doi.org/10.1016/j.soilbio.2020.107969>.
- Campo, J., Merino, A., 2016. Variations in soil carbon sequestration and their determinants along a precipitation gradient in seasonally dry tropical forest ecosystems. *Global Change Biology* 22, 1942–1956. <https://doi.org/10.1111/gcb.13244>.
- Chadwick, O.A., Gavenda, R.T., Kelly, E.F., Ziegler, K., Olson, C.G., Crawford Elliott, W., Hendricks, D.M., 2003. The impact of climate on the biogeochemical functioning of volcanic soils. *Chemical Geology* 202, 195–223. <https://doi.org/10.1016/j.chemgeo.2002.09.001>.
- Chang, R., Jin, T., Lü, Y., Liu, G., Fu, B., 2014. Soil carbon and nitrogen changes following afforestation of marginal cropland across a precipitation gradient in Loess Plateau of China. *PLoS One* 9, 1–12. <https://doi.org/10.1371/journal.pone.0085426>.
- Chen, C., Kukkadapu, R., Sparks, D.L., 2015. Influence of coprecipitated organic matter on Fe²⁺(aq)-Catalyzed transformation of ferrihydrite: implications for carbon dynamics. *Environmental Science and Technology* 49, 10927–10936. <https://doi.org/10.1021/acs.est.5b02448>.
- Cotrufo, M.F., Wallenstein, M.D., Boot, C.M., Denef, K., Paul, E., 2013. The Microbial Efficiency-Matrix Stabilization (MEMS) framework integrates plant litter decomposition with soil organic matter stabilization: do labile plant inputs form stable soil organic matter? *Global Change Biology* 19, 988–995. <https://doi.org/10.1111/gcb.12113>.
- Coward, E.K., Thompson, A.T., Plante, A.F., 2017. Iron-mediated mineralogical control of organic matter accumulation in tropical soils. *Geoderma* 306, 206–216. <https://doi.org/10.1016/j.geoderma.2017.07.026>.
- Derner, J.D., Schuman, G.E., 2007. Carbon sequestration and rangelands: a synthesis of land management and precipitation effects. *Journal of Soil and Water Conservation* 62, 77–85.
- Dictor, M.C., Tessier, L., Soulas, G., 1997. Reassessment of the K(ec) coefficient of the fumigation-extraction method in a soil profile. *Soil Biology and Biochemistry* 30, 119–127. [https://doi.org/10.1016/S0038-0717\(97\)00111-9](https://doi.org/10.1016/S0038-0717(97)00111-9).
- Domeignoz-Horta, L.A., Pold, G., Liu, X.J.A., Frey, S.D., Melillo, J.M., DeAngelis, K.M., 2020. Microbial diversity drives carbon use efficiency in a model soil. *Nature Communications* 11, 1–10. <https://doi.org/10.1038/s41467-020-17502-z>.
- Dynarski, K.A., Bossio, D.A., Scow, K.M., 2020. Dynamic stability of soil carbon: reassessing the “permanence” of soil carbon sequestration. *Frontiers in Environmental Science* 8. <https://doi.org/10.3389/fenvs.2020.514701>.
- Eusterhues, K., Wagner, F.E., Häusler, W., Hanzlik, M., Knicker, H., Totsche, K.U., Kögel-Knabner, I., Schwertmann, U., 2008. Characterization of ferrihydrite-soil organic matter coprecipitates by X-ray diffraction and Mössbauer spectroscopy. *Environmental Science and Technology* 42, 7891–7897. <https://doi.org/10.1021/es800881w>.
- Evans, S., Dieckmann, U., Franklin, O., Kaiser, C., 2016. Synergistic effects of diffusion and microbial physiology reproduce the Birch effect in a micro-scale model. *Soil Biology and Biochemistry* 93, 28–37. <https://doi.org/10.1016/j.soilbio.2015.10.020>.
- Fraser, F.C., Corstanje, R., Deeks, L.K., Harris, J.A., Pawlett, M., Todman, L.C., Whitmore, A.P., Ritz, K., 2016. On the origin of carbon dioxide released from

- rewetted soils. *Soil Biology and Biochemistry* 101, 1–5. <https://doi.org/10.1016/j.soilbio.2016.06.032>.
- Geyer, K., Schnecker, J., Grandy, A.S., Richter, A., Frey, S., 2020. Assessing microbial residues in soil as a potential carbon sink and moderator of carbon use efficiency. *Biogeochemistry* 151, 237–249. <https://doi.org/10.1007/s10533-020-00720-4>.
- Geyer, K.M., Kyker-Snowman, E., Grandy, A.S., Frey, S.D., 2016. Microbial carbon use efficiency: accounting for population, community, and ecosystem-scale controls over the fate of metabolized organic matter. *Biogeochemistry* 127, 173–188. <https://doi.org/10.1007/s10533-016-0191-y>.
- Giambelluca, W.T., Chen, Q., F. G.A., Price, P.J., Chen, Y.L., Chu, P.S., Eischeid, J.K., Delparto, M.D., 2013. Online rainfall atlas of Hawai'i. *Bulletin of the American Meteorological Society* 94, 313–316. <https://doi.org/10.1175/BAMS-D-11-00228.1>.
- Grant, K.E., Galy, V. v., Chadwick, O.A., Derry, L.A., 2019. Thermal oxidation of carbon in organic matter rich volcanic soils: insights into SOC age differentiation and mineral stabilization. *Biogeochemistry* 144, 291–304. <https://doi.org/10.1007/s10533-019-00586-1>.
- Grant, K.E., Galy, V. v., Haghypour, N., Eglinton, T.I., Derry, L.A., 2022. Persistence of old soil carbon under changing climate: the role of mineral-organic matter interactions. *Chemical Geology* 587, 120629. <https://doi.org/10.1016/j.chemgeo.2021.120629>.
- Gregorich, E.G., Gillespie, A.W., Beare, M.H., Curtin, D., Sanei, H., Yanni, S.F., 2015. Evaluating biodegradability of soil organic matter by its thermal stability and chemical composition. *Soil Biology and Biochemistry* 91, 182–191. <https://doi.org/10.1016/j.soilbio.2015.08.032>.
- Hall, S.J., Ye, C., Weintraub, S.R., Hockaday, W.C., 2020. Molecular trade-offs in soil organic carbon composition at continental scale. *Nature Geoscience* 13, 687–692. <https://doi.org/10.1038/s41561-020-0634-x>.
- Heckman, K., Hicks Pries, C.E., Lawrence, C.R., Rasmussen, C., Crow, S.E., Hoyt, A.M., von Fromm, S.F., Shi, Z., Stoner, S., McGrath, C., Beem-Miller, J., Berhe, A.A., Blankinship, J.C., Keiluweit, M., Marin-Spiotta, E., Monroe, J.G., Plante, A.F., Schimel, J., Sierra, C.A., Thompson, A., Wagai, R., 2022. Beyond bulk: density fractions explain heterogeneity in global soil carbon abundance and persistence. *Global Change Biology* 28, 1178–1196. <https://doi.org/10.1111/gcb.16023>.
- Huang, W., Hall, S.J., 2017. Elevated moisture stimulates carbon loss from mineral soils by releasing protected organic matter. *Nature Communications* 8. <https://doi.org/10.1038/s41467-017-01998-z>.
- Inagaki, T.M., Possinger, A.R., Grant, K.E., Schweizer, S.A., Mueller, C.W., Derry, L.A., Lehmann, J., Kögel-Knabner, I., 2020. Subsoil organo-mineral associations under contrasting climate conditions. *Geochimica et Cosmochimica Acta* 270, 244–263. <https://doi.org/10.1016/j.gca.2019.11.030>.
- Kaiser, K., Kalbitz, K., 2012. Cycling downwards - dissolved organic matter in soils. *Soil Biology and Biochemistry* 52, 29–32. <https://doi.org/10.1016/j.soilbio.2012.04.002>.
- Kallenbach, C.M., Grandy, A.S., Frey, S.D., Diefendorf, A.F., 2015. Microbial physiology and necromass regulate agricultural soil carbon accumulation. *Soil Biology and Biochemistry* 91, 279–290. <https://doi.org/10.1016/j.soilbio.2015.09.005>.
- Kleber, M., Eusterhues, K., Keiluweit, M., Mikutta, C., Mikutta, R., Nico, P.S., 2015. Mineral-organic associations: formation, properties, and relevance in soil environments. In: *Advances in Agronomy*. Elsevier Ltd, pp. 1–140. <https://doi.org/10.1016/bs.agron.2014.10.005>.
- Kleber, M., Sollins, P., Sutton, R., 2007. A conceptual model of organo-mineral interactions in soils: self-assembly of organic molecular fragments into zonal structures on mineral surfaces. *Biogeochemistry* 85, 9–24. <https://doi.org/10.1007/s10533-007-9103-5>.
- Kramer, M.G., Chadwick, O.A., 2018. Climate-driven thresholds in reactive mineral retention of soil carbon at the global scale. *Nature Climate Change* 8, 1104–1108. <https://doi.org/10.1038/s41558-018-0341-4>.
- Kramer, M.G., Sanderman, J., Chadwick, O.A., 2012. Long-term carbon storage through retention of dissolved aromatic acids by reactive particles in soil. *Global Change Biology* 18, 2594–2605. <https://doi.org/10.1111/j.1365-2486.2012.02681.x>.
- Kukkadapu, R.K., Zachara, J.M., Frederickson, J.K., Smith, S.C., Dohnalkova, A.C., Russell, C.K., 2003. Transformation of 2-line ferrihydrite to 6-line ferrihydrite under oxic and anoxic conditions. *American Mineralogist* 88, 1903–1914.
- Lehmann, J., Hansel, C.M., Kaiser, C., Kleber, M., Maher, K., Manzoni, S., Nunan, N., Reichstein, M., Schimel, J.P., 2020. Persistence of soil organic carbon caused by functional complexity. *Nature Geoscience* 13, 529–534. <https://doi.org/10.1038/s41561-020-0612-3>.
- Liang, C., Schimel, J.P., Jastrow, J.D., 2017. The importance of anabolism in microbial control over soil carbon storage. *Nature Microbiology* 2, 1–6. <https://doi.org/10.1038/nmicrobiol.2017.105>.
- Lynch, L.M., Machmuller, M.B., Cotrufo, M.F., Paul, E.A., Wallenstein, M.D., 2018. Tracking the fate of fresh carbon in the Arctic tundra: will shrub expansion alter responses of soil organic matter to warming. *Soil Biology and Biochemistry* 120, 134–144. <https://doi.org/10.1016/j.soilbio.2018.02.002>.
- Manzoni, S., Capek, P., Porada, P., Thurner, M., Winterdahl, M., Beer, C., Vico, G., Way, D., 2018. Reviews and Syntheses: Carbon Use Efficiency from Organisms to Ecosystems – Definitions, Theories, and Empirical Evidence 5929–5949.
- Manzoni, S., Taylor, P., Richter, A., Porporato, A., Ågren, G.I., 2012. Environmental and stoichiometric controls on microbial carbon-use efficiency in soils. *New Phytologist* 196, 79–91. <https://doi.org/10.1111/j.1469-8137.2012.04225.x>.
- Mason-Jones, K., Kuzyakov, Y., 2017. Non-metabolizable[®] glucose analogue shines new light on priming mechanisms: triggering of microbial metabolism. *Soil Biology and Biochemistry* 107, 68–76. <https://doi.org/10.1016/j.soilbio.2016.12.015>.
- Meier, I.C., Leuschner, C., 2010. Variation of soil and biomass carbon pools in beech forests across a precipitation gradient. *Global Change Biology* 16, 1035–1045. <https://doi.org/10.1111/j.1365-2486.2009.02074.x>.
- Miltner, A., Bombach, P., Schmidt-Brücken, B., Kästner, M., 2012. SOM genesis: microbial biomass as a significant source. *Biogeochemistry* 111, 41–55. <https://doi.org/10.1007/s10533-011-9658-z>.
- Noor, N., Thompson, A., 2022. Localized alteration of ferrihydrite natural organic matter coprecipitates following reaction with Fe(II). *Soil Science Society of America Journal* 1–11. <https://doi.org/10.1002/saj2.20366>.
- Öquist, M.G., Erhagen, B., Haei, M., Sparman, T., Ilsted, U., Schleucher, J., Nilsson, M. B., 2017. The effect of temperature and substrate quality on the carbon use efficiency of saprotrophic decomposition. *Plant and Soil* 414, 113–125. <https://doi.org/10.1007/s11104-016-3104-x>.
- Paul, E.A., Morris, S.J., Conant, R.T., Plante, A.F., 2006. Does the acid hydrolysis-incubation method measure meaningful soil organic carbon pools? *Soil Science of America Journal* 1035, 1023–1035. <https://doi.org/10.2136/sssaj2005.0103>.
- Pepe-Ranney, C., Campbell, A.N., Koechli, C.N., Berthrong, S., Buckley, D.H., 2016. Unearthing the ecology of soil microorganisms using a high resolution DNA-SIP approach to explore cellulose and xylose metabolism in soil. *Frontiers in Microbiology* 7, 1–17. <https://doi.org/10.3389/fmicb.2016.00703>.
- Perveen, N., Barot, S., Maire, V., Cotrufo, M.F., Shahzad, T., Blagodatskaya, E., Stewart, C.E., Ding, W., Siddiq, M.R., Dimassi, B., Mary, B., Fontaine, S., 2019. Universality of priming effect: an analysis using thirty five soils with contrasted properties sampled from five continents. *Soil Biology and Biochemistry* 134, 162–171. <https://doi.org/10.1016/j.soilbio.2019.03.027>.
- Plante, A.F., Fernández, J.M., Haddix, M.L., Steinweg, J.M., Conant, R.T., 2011. Biological, chemical and thermal indices of soil organic matter stability in four grassland soils. *Soil Biology and Biochemistry* 43, 1051–1058. <https://doi.org/10.1016/j.soilbio.2011.01.024>.
- Possinger, A.R., Bailey, S.W., Inagaki, T.M., Kögel-Knabner, I., Dynes, J.J., Arthur, Z.A., Lehmann, J., 2020. Organo-mineral interactions and soil carbon mineralizability with variable saturation cycle frequency. *Geoderma* 375, 114483. <https://doi.org/10.1016/j.geoderma.2020.114483>.
- Post, D.M., 2002. Using stable isotopes to estimate trophic position: models, methods, and assumptions. *Ecology* 83, 703–718. [https://doi.org/10.1890/0012-9658\(2002\)083\[0703:USITET\]2.0.CO;2](https://doi.org/10.1890/0012-9658(2002)083[0703:USITET]2.0.CO;2).
- Rasmussen, C., Heckman, K., Wieder, W.R., Keiluweit, M., Lawrence, C.R., Asefaw, A., Blankinship, J.C., Crow, S.E., Druhan, J.L., Hicks, C.E., Schimel, J.P., Alain, E.M., Christina, F.P., Berhe, A.A., Blankinship, J.C., Crow, S.E., Druhan, J.L., Hicks Pries, C.E., Marin-Spiotta, E., Plante, A.F., Schädel, C., Schimel, J.P., Sierra, C.A., Thompson, A., Wagai, R., 2018. Beyond clay: towards an improved set of variables for predicting soil organic matter content. *Biogeochemistry* 137, 297–306. <https://doi.org/10.1007/s10533-018-0424-3>.
- Roller, B.R.K., Schmidt, T.M., 2015. The physiology and ecological implications of efficient growth. *The ISME Journal* 9, 1481–1487. <https://doi.org/10.1038/ismej.2014.235>.
- Rumpel, C., Kögel-Knabner, I., 2011. Deep soil organic matter — a key but poorly understood component of terrestrial C cycle. *Plant and Soil* 338, 143–158. <https://doi.org/10.1007/s11104-010-0391-5>.
- Saiz, G., Bird, M.I., Domingues, T., Schrod, F., Schwarz, M., Feldpausch, T.E.D.R., Veenendaal, E., Lloyd, J.O.N., 2012. Variation in soil carbon stocks and their determinants across a precipitation gradient in West Africa. *Global Change Biology* 18, 1670–1683. <https://doi.org/10.1111/j.1365-2486.2012.02657.x>.
- Schmidt, M.W.I.L., Torn, M.S., Abiven, S., Dittmar, T., Guggenberger, G., Janssens, I.A., Kleber, M., Kögel-Knabner, I., Lehmann, J., Manning, D.A.C.C., Nannipieri, P., Rasse, D.P., Weiner, S., Trumbore, S.E., Kleber, M., Ko, I., 2011. Persistence of soil organic matter as an ecosystem property. *Nature* 478, 49–56. <https://doi.org/10.1038/nature10386>.
- Schneckenberger, K., Demin, D., Stahr, K., Kuzyakov, Y., 2008. Microbial utilization and mineralization of [14C]glucose added in six orders of concentration to soil. *Soil Biology and Biochemistry* 40, 1981–1988. <https://doi.org/10.1016/j.soilbio.2008.02.020>.
- Schuur, E.A.G., Matson, P.A., 2001. Net Primary Productivity and Nutrient Cycling across a Mesic to Wet Precipitation Gradient in Hawaiian Montane Forest, pp. 431–442. <https://doi.org/10.1007/s004420100671>.
- Schweizer, S.A., Hoeschen, C., Schlüter, S., Kögel-Knabner, I., Mueller, C.W., 2018. Rapid soil formation after glacial retreat shaped by spatial patterns of organic matter accrual in microaggregates. *Global Change Biology* 24, 1637–1650. <https://doi.org/10.1111/gcb.14014>.
- Shao, P., Lynch, L., Xie, H., Bao, X., Liang, C., 2021. Tradeoffs among microbial life history strategies influence the fate of microbial residues in subtropical forest soils. *Soil Biology and Biochemistry* 153, 108112. <https://doi.org/10.1016/j.soilbio.2020.108112>.
- Six, J., Bossuyt, H., Degryze, S., Denef, K., 2004. A history of research on the link between (micro)aggregates, soil biota, and soil organic matter dynamics. *Soil and Tillage Research* 79, 7–31. <https://doi.org/10.1016/j.still.2004.03.008>.
- Thompson, A., Rancourt, D.G., Chadwick, O.A., Chorover, J., 2011. Iron solid-phase differentiation along a redox gradient in basaltic soils. *Geochimica et Cosmochimica Acta* 75, 119–133. <https://doi.org/10.1016/j.gca.2010.10.005>.
- Torn, M.S., Trumbore, S.E., Chadwick, O.A., Vitousek, P.M., Hendricks, D.M., 1997. Mineral control of soil organic carbon storage and turnover. *Nature* 389, 171–173.
- Unger, S., Máguas, C., Pereira, J.S., David, T.S., Werner, C., 2010. The influence of precipitation pulses on soil respiration - assessing the "Birch effect" by stable carbon isotopes. *Soil Biology and Biochemistry* 42, 1800–1810. <https://doi.org/10.1016/j.soilbio.2010.06.019>.
- Vogel, C., Mueller, C.W., Höschen, C., Buegger, F., Heister, K., Schulz, S., Schloter, M., Kögel-Knabner, I., 2014. Submicron structures provide preferential spots for carbon

- and nitrogen sequestration in soils. *Nature Communications* 5, 1–7. <https://doi.org/10.1038/ncomms3947>.
- Weintraub, M.N., Scott-Denton, L.E., Schmidt, S.K., Monson, R.K., 2007. The effects of tree rhizodeposition on soil exoenzyme activity, dissolved organic carbon, and nutrient availability in a subalpine forest ecosystem. *Oecologia* 154, 327–338. <https://doi.org/10.1007/s00442-007-0804-1>.
- Whitman, T., Neurath, R., Perera, A., Chu-Jacoby, I., Ning, D., Zhou, J., Nico, P., Pett-Ridge, J., Firestone, M., 2018. Microbial community assembly differs across minerals in a rhizosphere microcosm. *Environmental Microbiology*. <https://doi.org/10.1111/1462-2920.14366>.
- Woolf, D., Lehmann, J., 2019. Microbial models with minimal mineral protection can explain long-term soil organic carbon persistence. *Scientific Reports* 9, 6522. <https://doi.org/10.1038/s41598-019-43026-8>.